Available online at www.sciencedirect.com
ScienceDirect
Cement & Concrete Composites 29 (2007) 575–581
Cement & Concrete Composites
www.elsevier.com/locate/cemconcomp

A quantitative study on the plastic shrinkage cracking in high strength hybrid fibre reinforced concrete

A. Sivakumar, Manu Santhanam *

Department of Civil Engineering, Indian Institute of Technology, Madras, India

Received 13 January 2006; received in revised form 16 November 2006; accepted 15 March 2007
Available online 27 March 2007

Abstract

High strength concrete using silica fume is prone to plastic shrinkage cracking in dry and windy conditions. Addition of fibres is known to restrict the growth of shrinkage cracks. The present study was aimed at controlling plastic shrinkage cracks in high strength silica fume concrete by means of adding fibre reinforcement up to 0.5% by volume of concrete. Individual steel fibres as well as hybrid combinations of steel and non-metallic (polyester, polypropylene and glass) fibres were evaluated for their influence on plastic shrinkage cracking. Results showed that hybrid fibres were most effective in reducing shrinkage cracks. Among the hybrid fibre combinations, the steel and polyester combination was found to reduce plastic shrinkage cracks by more than 99% compared to the plain concrete. Increased fibre availability and low stress levels at early ages were the main factors contributing to the good performance of hybrid fibre mixtures.

Keywords: Hybrid fibres; Plastic shrinkage; High strength concrete

1. Introduction

Three-dimensional volume changes in fresh concrete occur primarily due to rapid loss of surface bleed water on evaporation. This results in the rapid drawdown in pore water level, causing an increase in pore water pressure, which tends to bring the neighboring solid particles closer [1]. All this leads to shrinking of cement paste; the resultant restraint offered by aggregates leads to cracking on the surface of fresh concrete [2]. Plastic shrinkage cracks are typically observed in thin concrete elements with a high surface area to volume ratio. High performance concretes, with low water to cement ratio, and incorporating silica fume, due to the minuteness of pores formed and reduced bleeding rate, are more prone to plastic shrinkage cracking [3]. Fresh concrete is susceptible to plastic shrinkage cracking especially during hot, windy, and dry weather conditions [4]. When the evaporation rate is significantly higher than bleeding rate, it can cause high tensile stresses to develop in the capillary pores in the surface zone of concrete that may be sufficient to exceed the tensile strength of concrete, especially at early ages [5,6]. If the surface cracks that develop as a result of plastic shrinkage remain unnoticed, they become channels for passage of external deteriorating agents and reduce long-term durability [7].

Precautions against plastic shrinkage cracking include preventing rapid drying of the surface of concrete and adopting good curing practices. Besides these, the use of fibres as a secondary reinforcing mechanism can help in mitigating the stresses developed upon drying [8]. The addition of metallic fibres has been reported to provide adequate tensile strength to concrete in addition to controlling shrinkage cracks [9,10]. Moreover, the addition of non-metallic fibres such as polypropylene, glass, polyethylene, etc. is reported to reduce drying shrinkage crack widths of concrete at later ages [11].

At present, there are no standard testing methods to characterize plastic shrinkage cracking in plain and fibre reinforced concretes. Various specimen geometries have been used in the past to simulate a realistic condition of

* Corresponding author. Tel.: +91 44 22574283; fax: +91 44 22570509.
E-mail address: manus@iitm.ac.in (M. Santhanam).

0958-9465/$ - see front matter © 2007 Elsevier Ltd. All rights reserved.
doi:10.1016/j.cemconcomp.2007.03.005

plastic shrinkage cracking. This includes slabs with stress concentrators [12–14], rings [15], a modified beam test [16], and slabs with realistic substructures [17]. Some of the measurement techniques reported in the above tests use randomly selected locations over a large cracked surface to assess the cracking potential. In addition, conducting accurate manual measurement of the entire cracked area is rather complex and cumbersome. The crack measurements reported also involve cumbersome calculations, and the use of average crack width at selected locations sometimes leads to erroneous interpretation. Image analysis of the cracked area is reported to be more appropriate than manual crack measurement to study cracking at different scales [18]. With the use of image analysis, it has become easier to monitor the crack development [19] and microstructure [20] of cementitious systems.

In this paper, an attempt has been made to study the synergistic behavior of hybrid combinations of steel and non-metallic fibres in controlling plastic shrinkage cracks. Using an advanced image analysis technique, a reliable estimation of various crack measurements has been made. This provides a systematic approach for quantifying the effect of fibre reinforcement on plastic shrinkage cracking.

2. Materials and experimental methods

2.1. Materials used

Ordinary Portland cement conforming to IS 12269 [21] and silica fume, obtained from Elkem Materials, India, was used for the concrete mixtures. River sand with a specific gravity of 2.65 and fineness modulus of 2.64 was used as the fine aggregate, while crushed granite of specific gravity 2.82 was used as coarse aggregate. A naphthalene sulphonate based superplasticizer was used to obtain the desired workability. The fibres used in the study were hooked steel, polypropylene, polyester, and glass, obtained from local manufacturers.

2.2. Mixture proportioning

Trial mixtures were prepared to obtain target strength of 60 MPa at 28 days, along with a workability of 75–120 mm. In order to obtain the desired workability, only the superplasticizer dosage was varied. The detailed mixture proportions for the study are presented in Table 1, while the properties and volume fractions of various fibres used in the mixtures are given in Tables 2 and 3.

2.3. Mixing and placing

Concrete was mixed using a rotary pan mixer of 100 kg capacity. The coarse aggregate, fine aggregate, cement, and silica fume were first mixed dry for a period of 2 min. The superplasticizer was then mixed thoroughly with the mixing

Table 1
Concrete mixture proportions (for all mixtures) used in the study

Cement (kg/m^3)	Silica fume (kg/m^3)	Fine aggregate (kg/m^3)	Coarse aggregate (kg/m^3)		Water (kg/m^3)	Superplasticizer (kg/m^3)
			10 mm	20 mm		
372	28	750	570	570	160	8

Table 2
Properties of the different fibres used

Property	Hooked steel	Polypropylene	Glass	Polyester
Length (mm)	30	20	6	12
Diameter (mm)	0.5	0.10	0.01	0.05
Aspect ratio (l/d)	60	200	600	240
Specific gravity	7.8	0.9	2.72	1.35
Tensile strength (MPa)	1700	450	2280	970
Elastic modulus (GPa)	200	5	80	15
Failure strain (%)	3.5	18	3.6	35

Table 3
Dosage of different fibre combinations used in the study

Mix ID	Volume fraction of hooked steel (%)	Volume fraction of non-metallic fibre (%)	Fibre dosage (kg/m^3)				Total fibre dosage (kg/m^3)
			S	PP	PO	G	
C1	0	–	–	–	–	–	–
HST2	0.5		38.98		–	–	38.98
HSPP3	0.38	0.12	27.22	1.34			28.56
HSPO4	0.38	0.12	27.22		1.82		29.04
HSGL5	0.38	0.12	27.22			3.84	31.06
HSPP6	0.25	0.25	19.44	2.26	–	–	21.70
HSPO7	0.25	0.25	19.44	–	3.36	–	22.80
HSGL8	0.25	0.25	19.44	–	–	6.77	26.21
HSPP9	0.12	0.38	9.36	3.41	–	–	12.77
HSPO10	0.12	0.38	9.36	–	5.14	–	14.50
HSGL11	0.12	0.38	9.36	–	–	10.32	19.68
PP12	–	0.5	–	4.5	–	–	4.50
PO13	–	0.5	–	–	6.72	–	6.72
GL14	–	0.5	–	–	–	13.63	13.63

Note: S – steel fibre, PP – polypropylene fibre, PO – polyester fibre, and G – glass fibre.

water and added to the mixer. Fibres were dispersed by hand in the mixture to achieve a uniform distribution throughout the concrete, which was mixed for a total of 4 min. After mixing, the workability of concrete was determined using three methods: slump [22], inverted slump [23] and Vebe consistometer test [24]. The concrete was placed in the fabricated mould kept on a table vibrator. A smooth steel trowel was used to finish the fresh concrete. Thirty minutes from the time when water added to the mixer, the specimens were transferred to the environmental chamber.

2.4. Specimen dimensions and environmental conditions

The slab mould (see Fig. 1) of dimension $500 \times 250 \times 75$ mm was made of laminated board. A thin polyethylene sheet was placed over the base to eliminate base friction between the concrete and laminated board. The slab was provided with a stress riser of 55 mm height at the center and two base restraints of 35 mm height at 35 mm from both ends, along the transverse direction. In addition to this, a bolt and nut arrangement was provided at the ends to restrict the longitudinal movement of the concrete slab from the edges and to provide additional restraint, increasing the potential of cracking at the notch. The concrete slabs were stored after casting in an environmental chamber with dimensions of $2.75 \times 0.9 \times 0.9$ m, as shown in Fig. 2. Apart from controlling temperature and humidity, this chamber was equipped with a high-speed fan of air velocity 3.8 m/s fixed on the walls of the chamber to accelerate drying of concrete. The slabs were exposed to a constant temperature of 35 ± 1 °C, a relative humidity of $40 \pm 1\%$, a wind velocity of 6 m/s. The evaporation rate, measured by detecting the loss of water from a porcelain bowl placed inside the chamber, was 0.62 kg/m^2/h. The slabs were checked visually for any signs of cracking at approximately 30-min intervals. The slabs (inside the moulds) were kept in the chamber for 24 h.

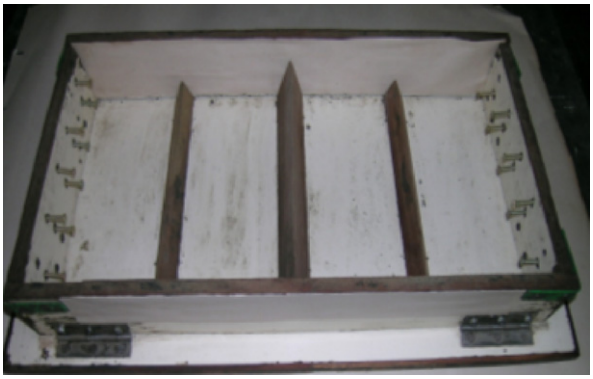

Fig. 1. Fabricated mould setup.

Fig. 2. Environmental chamber used for storage of specimens.

3. Results

3.1. Crack observations

The time of occurrence of first crack was noted for all slabs during the experiments. In the case of plain concrete, approximately 160 min after mixing with water, a fine hairline crack running throughout the width of the slab was observed above the central stress riser. This fine crack, which could have possibly been caused due to settlement, was found to widen upon further drying. In the case of fibre reinforced concrete specimens, the appearance of the first crack took a relatively longer time (more than 7 h). This could be attributed to the availability of bleed water on the top surface, which delays drying of the surface. Fibres in concrete have been reported to act as bleeding channels, which supply water to replenish the drying surface and reduce the magnitude of capillary stresses developed [25].

In the case of plain concrete, a single crack over the central stress riser was found to run almost straight throughout the width of the specimen. However, for fibre

Fig. 3. Plastic shrinkage crack in the plain concrete (C1) slab (area 250×250 mm).

concretes the crack was rather short, discontinuous and took a tortuous path around aggregate pieces or along fibres. In addition, some hairline cracks were noticed to branch out from the main cracks in the case of hybrid fibre concretes.

3.2. Crack measurements

The crack measurements comprise of the crack length, crack width (maximum and average) and total crack area. Images of the crack were captured using an optimal zoom camera based on crack visibility; some captured images of different concrete specimens are shown in Figs. 3–7, and calibration of the image size using a ruler is shown in Fig. 8. Subsequently, the captured images were processed and edited with image analysis software to get a clear crack profile using various mathematical operations such as binarization, thresholding, cleaning and filtering. An example of an image after the processing operations is given in Fig. 9.

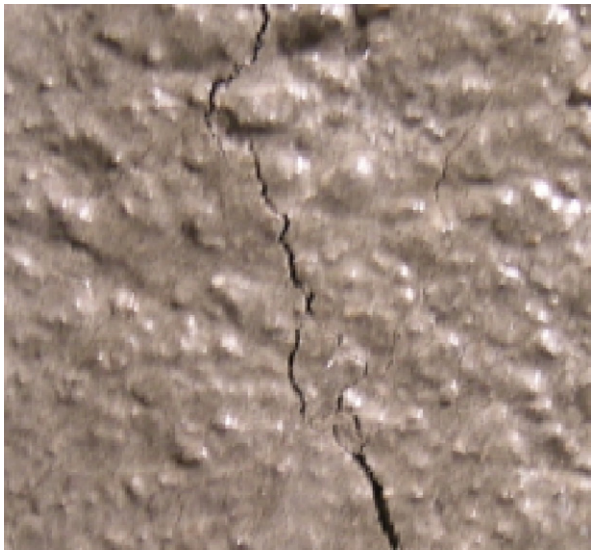

Fig. 4. Plastic shrinkage crack in the steel fibre concrete (HST2) slab (area 75×75 mm).

Fig. 5. Plastic shrinkage crack in the steel–polypropylene hybrid concrete (HSPP3) slab (area 35×35 mm).

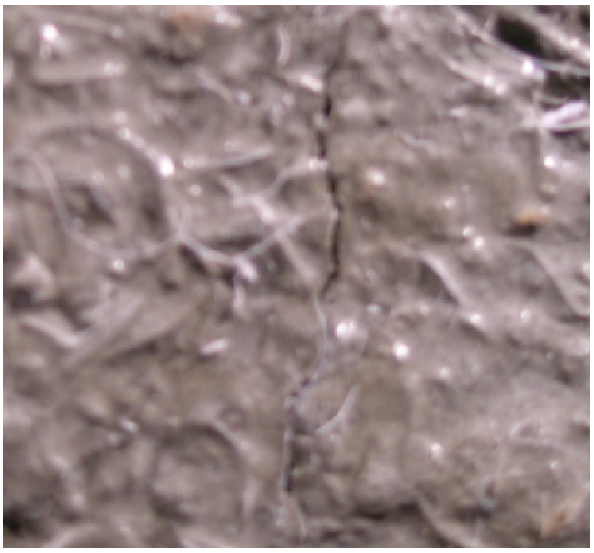

Fig. 6. Plastic shrinkage crack in the steel–polyester hybrid concrete (HSPO4) slab (area 18×18 mm).

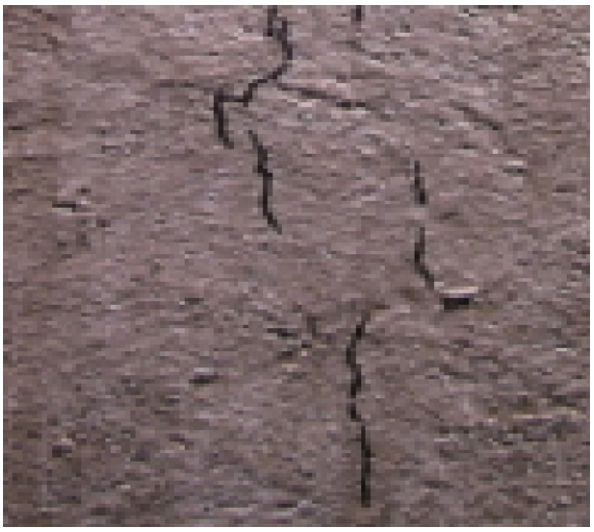

Fig. 7. Secondary crack observed in steel–glass hybrid concrete (HSGL5) slab (area 52×52 mm).

The length of crack was determined by using a curve-tracing tool in the image analysis software to trace the crack. The length was then calculated in terms of pixels, which were converted to length units (mm) using the calibration scale. Similarly, using a linear scale tool in the image analysis software, the crack width was calculated at 180 equi-distant points along the crack. The actual image resolution varied due to variation in height at which pictures were taken based on the crack visibility. The total crack area was then calculated on the binarized image

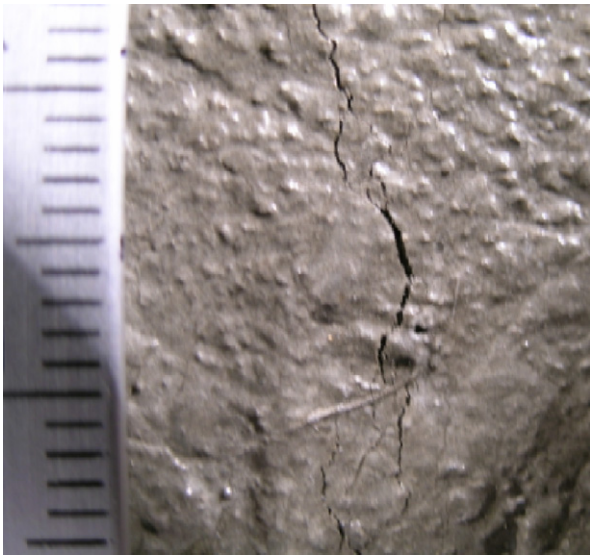

Fig. 8. Calibration of measurement using graduated scale.

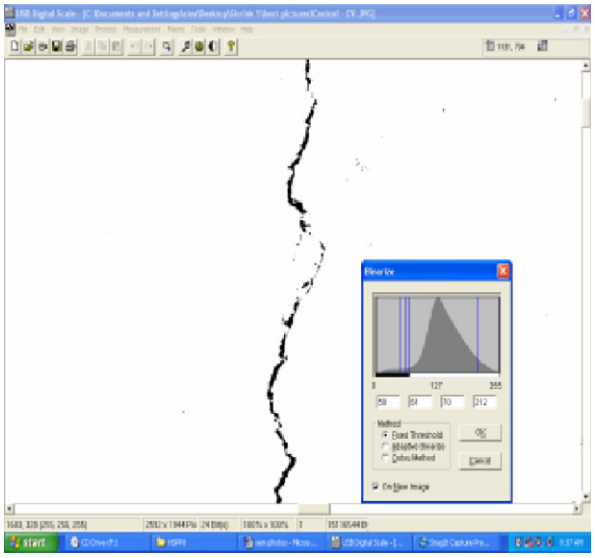

Fig. 9. Example of a processed image of controlled concrete.

using the software. In the case of very fine cracks, the crack widths and length were recorded using a crack width comparator, which can measure from 0.025 to 0.25 mm. The results are presented in Table 4.

4. Discussion of experimental results

Experimental results given in Table 4 indicate that the maximum crack width was observed in the case of plain concrete; with fibre addition, the crack widths were reduced. Compared to steel fibre concrete, hybrid fibre concretes showed better crack control features. The total crack area reduced with increased addition of non-metallic fibres, as shown in Fig. 10. The reduction in crack width using hybrid fibre combinations (presented in Table 4) significantly contributed to the reduction of the overall crack area. The improved performance of hybrid fibre combinations can be attributed to the increase in fibre availability compared to the steel fibre concrete, since all non-metallic fibres had considerably lower specific gravity than steel. The increase in fibre availability reduces the fibre spacing and also the propensity for crack origination. However, the performance is not linked only to the fibre availability (which in this study has been characterized by the reinforcement index in Table 4). Amongst the hybrid fibre concretes, the performance was further affected by the length and stiffness of the non-metallic fibres. Polyester and polypropylene fibres performed better than glass. An explanation for this trend could be the differences in stiffness of these fibres. Polyester and polypropylene, which have a much lower elastic modulus than glass (see Table 2), are probably more effective in restricting plastic shrinkage

Table 4
Experimental results of crack measurements

Type of concrete	Mix ID	Volume fraction of fibre (%)	Reinforcement index ($W_f \times L/d$)	Time of first crack appearance (min)	Maximum crack width (mm)	Total crack length (mm)	Total crack area (mm^2)	Percentage reduction in crack area
Plain concrete	C1	0	–	160	0.541	301.62	151.11	–
Steel fibre	HST2	0.5	2338	280	0.416	249.83	77.69	48.58
Steel + polypropylene fibre	HSPP3	0.38 + 0.12	1855	360	0.285	239.84	29.98	80.16
Steel + polypropylene fibre	HSPP6	0.25 + 0.25	1541	420	0.174	217.20	16.29	89.21
Steel + polypropylene fibre	HSPP9	0.12 + 0.38	1127	–	0.134	95.45	4.96	96.71
Polypropylene fibre	PP12	0.5	747	–	0.080	48.65	1.80	98.80
Steel + polyester fibre	HSPO4	0.38 + 0.12	1906	540	0.211	146.47	14.93	90.11
Steel + polyester fibre	HSPO7	0.25 + 0.25	1670	600	0.173	104.75	7.22	95.21
Steel + polyester fibre	HSPO10	0.12 + 0.38	1332	–	0.124	51.44	2.31	98.46
Polyester fibre	PO13	0.5	1008	–	0.081	6.23	0.18	99.87
Steel + glass fibre	HSGL5	0.38 + 0.12	3937	300	0.362	271.91	59.82	60.41
Steel + glass fibre	HSGL8	0.25 + 0.25	5228	360	0.261	189.48	33.15	78.05
Steel + glass fibre	HSGL11	0.12 + 0.38	6753	420	0.195	117.46	15.38	89.81
Glass fibre	GL14	0.5	8178	–	0.130	53.19	4.94	96.72

Note: – denotes that time of occurrence could not be detected due to fine hairline cracks.

cracks, where the stress levels causing cracking are quite low. In addition, the polyester and polypropylene fibres are much longer compared to glass fibres (that have a length of only 6 mm); the short glass fibres could have got pulled out of the matrix even at the low stress levels, as the bond between the fibre and matrix would not have developed sufficiently. The steel–polyester combination performed the best among the three hybrid fibre combinations.

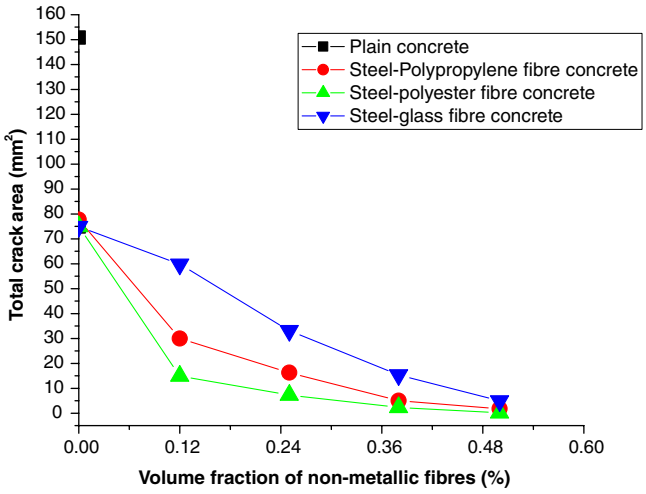

Fig. 10. Influence of dosage of non-metallic fibres on total crack area.

Although the increase in non-metallic fibres resulted in an appreciable crack width reduction, it also caused a decrease in workability of concrete (presented in Table 5). The reduced workability could be attributed to the larger number of fibres available (since non-metallic fibres have a lower specific gravity) that causes balling and resultant trapping of free water. This resulted in harsh mixtures that required high compaction energy. This negative effect restricts the maximum dosage of polypropylene and polyester fibres to an optimal level of 0.25% (V_f) based on the workability range of 50–75 mm. However, in the case of glass fibres the increase in dosage up to 0.38% does not affect the workability.

Table 5
Workability of various concrete mixes

Mix ID	Volume fraction of hooked steel (%)	Volume fraction of non-metallic fibre (%)	Inverted slump flow time (s)	Vebe time (s)	Slump (mm)
C1		–	2	–	105
HST2	0.5	–	11	1	80
HSPP3	0.38	0.12	15	3	75
HSPO4	0.38	0.12	18	5	70
HSGL5	0.38	0.12	13	2	80
HSPP6	0.25	0.25	20	7	65
HSPO7	0.25	0.25	27	10	55
HSGL8	0.25	0.25	19	3	70
HSPP9	0.12	0.38	45	17	35
HSPO10	0.12	0.38	53	25	Stiff mix
HSGL11	0.12	0.38	32	16	50
PP12	–	0.5	50	19	Stiff mix
PO13	–	0.5	62	36	Stiff mix
GL14	–	0.5	41	16	Stiff mix

Table 6
Crack statistics for the different concrete mixtures

Mix ID	Mean crack width (mm)	Standard deviation	Coefficient of variation (%)	Percentage of crack widths					
				0.547–0.4 mm	0.4–0.3 mm	0.3–0.2 mm	0.2–0.1 mm	0.1–0.05 mm	0.05–0.025 mm
C1	0.501	0.162	32.3	80	12	5	3		
HST2	0.311	0.132	42.3	45	10	15	20	9	1
HSPP3	0.125	0.081	64.8	–	–	25	23	25	27
HSPP6	0.075	0.012	16.8	–	–	–	27	35	38
HSPP9	0.052	0.018	33.6	–	–	–	34	45	21
PP12	0.037	0.075	15.0	–	–	–	–	86	14
HSPO4	0.102	0.021	20.5	–	–	43	27	26	4
HSPO7	0.069	0.035	50.7	–	–	–	34	45	21
HSPO10	0.045	0.021	44.4	–	–	–	15	57	28
PO13	0.030	0.011	36.6	–	–	–	–	44	56
HSGL5	0.220	0.052	23.5	–	17	23	47	10	3
HSGL8	0.175	0.063	36.0	–	–	34	56	5	5
HSGL11	0.131	0.192	37.9	–	–	–	32	34	34
GL14	0.093	0.027	29.1	–	–	–	17	23	60

In the case of polyester and polypropylene hybrid fibre concretes, at high volume fractions of non-metallic fibres, secondary cracks were seen to appear branching out from the main crack. These secondary cracks were thinner than the main crack (crack widths were less than 0.035 mm). The total area of secondary cracks was calculated to be always less than 10% of main cracks. As the non-metallic fibre fraction increased to 0.38%, the main crack was neither continuous nor distinctive. This trend was slightly different for steel–glass fibre concretes, as the secondary crack widths were of the order of 0.075 mm.

The crack statistics are presented in Table 6. The percentage of cracks of different sizes indicates the degree of cracking. The percentage of crack widths greater than 0.3 mm was found to be more than 90% in the case of controlled concrete and 60% in the case of steel fibre concrete and almost zero in the case of hybrid fibre concretes (except for the steel–glass combination at low volume fraction of glass fibres). In the case of hybrid fibre concretes, the percentage of cracks lesser than 0.05 mm was maximum at increased levels of non-metallic fibre reinforcement.

5. Conclusions

This paper reported experimental results of plastic shrinkage studies conducted on high strength silica fume concrete incorporating hybrid combinations of fibres. The following conclusions can be drawn from the results presented in this paper:

1. Plastic shrinkage cracks were reduced significantly by fibre addition (by 50–99% compared to plain concrete without fibres); hybrid fibres were more effective in crack reduction compared to individual steel fibres.
2. Among the three hybrid fibre combinations, the steel–polyester combination caused the best crack reduction of 99% compared to plain concrete.
3. With an increase in the non-metallic fibre content, even though the crack characteristics were significantly improved, the concrete mixtures had poor workability. This effectively restricts the maximum content of non-metallic fibres to 0.25% (volume fraction).
4. Secondary cracks were observed branching out from the main crack in the case of hybrid fibre concrete specimens.
5. Among the three hybrid fibre combinations, the steel–glass combination did not perform as well as the other two, possibly because the stiff glass fibres were not able to contribute much at the low stress levels causing early age cracking.

References

[1] Wittmann FH. On the action of capillary pressure in fresh concrete. Cem Concr Res 1976:49–56.
[2] Balaguru P, Shah SP. Fiber reinforced cement composites. New York: McGraw-Hill; 1992. 535–76.
[3] Balaguru P. Contribution of fibers to crack reduction of cement composites during the initial and final setting period. ACI Mat J 1994:280–8.
[4] Grzybowski M, Shah SP. Shrinkage cracking of fiber reinforced concrete. ACI Mat J 1990:138–48.
[5] Cohen MD, Olek J, Dolch WL. Mechanism of plastic shrinkage cracking in portland-cement and portland cement–silica fume paste and mortar. Cem Concr Res 1990;1(20):103–19.
[6] Wang K, Jansen D, Shah SP. Permeability of cracked concrete. Cem Concr Res 1997;4(27):409–15.
[7] Johansen R, Dahl PA. Control of plastic shrinkage in concrete at early ages. In: Proceedings of the eighteenth conference on our world in concrete and structures, Singapore, 1993. p. 149–54.
[8] Soroushian P, Mirza F, Alhozaimy A. Plastic shrinkage cracking of polypropylene fiber-reinforced concrete slabs. Transport Res Rec 1993:69–72.
[9] Banthia N, Yan C. Shrinkage cracking in polyolefin fiber-reinforced concrete. ACI Mat J 2000:432–7.
[10] Ramakrishnan V. Concrete plastic shrinkage reduction potential of synergy fibers, In: Symposium of the eightieth annual transportation research board meeting, Washington, DC, 2001.
[11] Nanni A, Ludwig DA, Mcgillis MT. Plastic shrinkage cracking of restrained fiber-reinforced concrete. Transport Res Rec 1993(1382): 69–72.
[12] Kraai PP. Proposed test to determine the cracking potential due to drying shrinkage of concrete. Concrete Constr 1985;9(30):775–8.
[13] Berke NS, Dalliare MP. The effect of low addition rate of polypropylene fibers on plastic shrinkage cracking and mechanical properties of concrete. Fiber reinforced concrete: development and innovations 1994; ACI SP-142-2: 19–41.
[14] Weiss WJ, Yang W, Shah SP. Factors influencing durability and early-age cracking in high-strength concrete structures. ACI-SP 189 2001; ACI SP-189-22: 387–409.
[15] Wang KJ, Shah SP, Phuaksuk P. Plastic shrinkage cracking in concrete materials – influence of fly ash and fibers. ACI Mat J 2001; 11(98):458–64.
[16] Mora J, Gettu R, Olazábal C, Martín MA, Aguado, AA. Effect of the incorporation of fibers on the plastic shrinkage of concrete, Fiber-Reinforced Concretes (FRC), BEFIB'2000 (Lyon, France), RILEM Publications, S.A.R.L., Cachan, France, p. 705–14.
[17] Banthia N, Yan C, Mindess S. Restrained shrinkage cracking in fiber reinforced concrete: a novel test technique. Cem Concr Res 1996; 1(26):9–14.
[18] Chermant J-L. Why automatic image analysis? An introduction to this issue. Cem Concr Comp 2001;4(23):127–31.
[19] Mindess S, Diamond S. A preliminary SEM study of crack-propagation in mortar. Cem Conc Res 1980(10):509–19.
[20] Diamond S, Bonen D. A Re-evaluation of hardened cement paste microstructure based on backscattered SEM investigations. Materials research society symposium proceedings 1995(370):13–22.
[21] Indian Standard Designation, IS 12269-1987, Specification for 53 grade ordinary portland cement, Bureau of Indian Standards, New Delhi, India.
[22] ASTM Standard Designation C 143-90a, Standard test method for slump of hydraulic cement concrete, Annual book of ASTM standards, vol 4.02, Pennsylvania, United states.
[23] ASTM Standard Designation C 995-94, Standard test method for time of flow of fiber-reinforced concrete through inverted slump cone, Annual book of ASTM standards, vol 4.02, Pennsylvania, United States.
[24] ASTM Standard Designation C 1170, Vebe consistometer for roller-compacted concrete, Annual book of ASTM standards, vol 4.02, Pennsylvania, United States 4.02, 533–40, Pennsylvania, United States.
[25] Zollo RF, Alter J, Bouchacourt B. Plastic and drying shrinkage in concrete containing collated fibrillated polypropylene fibers. In: Proceedings of RILEm third international symposium on development in fiber reinforced cement and concrete 1986, England.